# THE MID-TERM QUASI-PERIODICITIES OF SUNSPOT GROUP FLUCTUATIONS

*R. GETKO, Astronomical Institute, Wrocław University, Kopernika 11, 51--622 Wrocław, Poland, getko @astro.uni.wroc.pl*

**Abstract**

**The existence of the mid-term periodicities in sunspot data from the solar cycle 19 is considered. Although the auto-correlation and the spectral analyses of sunspot activity fluctuations show the domination of the 10-rotation quasi-periodicity, the regression and the wavelet analyses for the Wolf number fluctuations indicate that it is not possible to find one mid-term periodicity (from 4 to 14 rotations) during the whole solar cycle. The sunspot group clusters from cycle 19 are used to find the longitudinal zones in which the mid-term periodicities exist. The division of each solar hemisphere into 30º-wide longitude bins and the wavelet calculations for the areas of sunspot clusters belonging to these 30º bins enable one to detect from 1 to 3 longitudinal zones at the same time. These zones are detected during the high-activity period (73 rotations for the northern hemisphere and 81 rotations for the southern hemisphere). The shorter periods (from 4 to 7 rotations) are also detected.**

**Keywords: Wolf number fluctuations, sunspot area fluctuations, autocorrelation function, periodogram, wavelets, regression**

## 1.Introduction

The occurrence of the mid-term periodicities (from 4 to 30 rotations) in the sunspot data from the whole solar disk or from each of solar hemisphere was investigated by many researchers. The most common are discussed the about 6-rotation (155-day) and the about 10-rotation (270-day) periodicities. In addition to these lists are also two longer: the about 17-rotation (460-day) and the about 23-rotation (620-day) periodicities. A more up to date review is given by Obridko and Shelting (2007). However, Getko (2009) showed that these periodicities could be treated as subharmonics of the 10-rotation period. This fact could explain a wide range of periodicities in various solar indices at all levels from the tachocline to the Earth.

The main goal of this paper is to explain the problem of occurrence of these periodicities for one selected solar cycle. For this study the most active solar cycle (No. 19) was chosen. For Wolf sunspot number fluctuations the comparison between the peaks of the periodogram, the auto-correlation function and the global wavelet power enables one to deduce the prominent periodicities. The temporal behavior of these periodicities can be described by both the wavelet map and the regression analysis. Such an analysis could indicate that these periodicities exist in the whole solar cycle or in a part of it. The N - S asymmetry of solar activity (Vizoso and Ballester, 1990) suggests that the both hemispheres should be considered separately. Thus, the auto-correlation, the power spectrum and the wavelet analyses of the sunspot-area fluctuations from each solar hemisphere can explain the similarities or the differences between the dominant periodicities in both the solar hemispheres. To associate these results with the observed

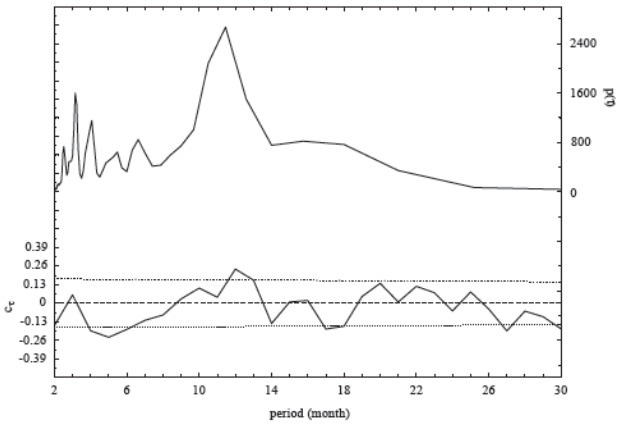


*Figure 1.* The upper curve shows the periodogram of the Wolf number fluctuations $\{F_i\}_{i=1}^{M}$ for cycle 19. The scale for the periodogram values is presented on the right axis. The lower curve presents the auto-correlation function. The dotted lines represent two standard errors of the auto-correlation function. The dashed horizontal line shows the zero level. The scale for the auto-correlation values is shown on the left axis.

features on the solar surface, the longitude distributions of sunspot group clusters that are close to one another and that create the strong sunspot-area fluctuations that

existed during each solar cycle in each solar hemisphere were evaluated (Getko, 2014). Because such clusters have a longitudinal extent up to 30° (Getko, 2007), the solar disk is divided into 30°-wide longitude bins. For each longitude bin the new sunspot-area time series is considered. It contains all sunspot groups or sunspot-group clusters that existed during each solar cycle. Its wavelet analysis determines the time intervals where the mid-term periodicities exist.

## 2. The Data

Several sunspot data sets for the years 1954-1964 (cycle 19) have been taken to analyse the mid-term periodicities (for period from 4 to 14 months). These include the mean monthly Wolf numbers, the mean sunspot areas from the southern and the northern hemispheres calculated for each Carrington rotation (about 27 days) and the areas of sunspot clusters and single sunspot groups belonging to the 30°-wide longitude bins from each solar hemisphere separately.
The mean monthly Wolf numbers for the years 1954-1964 (cycle 19) are available in web pages of Solar Influences Data Analysis Center (SIDC) {http://sidc.oma.be/sunspot-data/}. To remove the 11-year cycle the moving average of the monthly Wolf numbers is used. As a result the fluctuation $(F_i)$ of the monthly Wolf number $(R_i)$ from the consecutively smoothed monthly Wolf number $(\overline{R_i})$ is obtained:

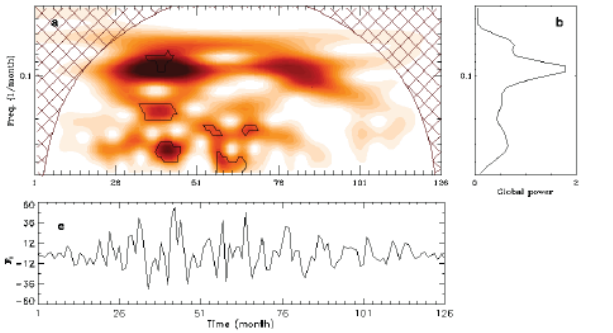


*Figure 2.* a: Wavelet power spectrum of $\{F_i\}_{i=1}^{M}$ mapping a time-frequency evolution of about 11-month periodicity. Top values of wavelet power are denoted by gradual darkening. Black contours denote significance levels of 95% for detected peaks. A cone of influence is marked by the dashed region. b: Time series $\{F_i\}_{i=1}^{M}$. c: Corresponding global wavelet power spectrum.

$$F_i = R_i - \overline{R_i} \quad \text{for } i = 1,...,M,$$

where $\overline{R_i} = \frac{1}{13}\sum_{j=i-6}^{i+6} R_j$ is the 13-months running mean. The time series $\{F_i\}_{i=1}^{M}$ (Figure 2c) contains $M = 126$ elements.
To obtain the sunspot areas per Carrington rotation the daily sunspot areas for the northern hemisphere $(D_l^n)$, and the southern hemisphere $(D_l^s)$ from web pages of National Data Geophysical Center (NGDC) (http://www.ngdc.noaa.gov/stp/solar/) are used. For the i-th Carrington rotation the mean area for the northern hemisphere $(S_i^n)$ is given by $S_i^n = \frac{1}{K}\sum_{l=1}^{K} D_l^n$, where $K$ is the number of days for the i-th rotation. Similarly to the Wolf numbers, the fluctuation $(F_i^n)$ of the mean area $(S_i^n)$ from the smoothed mean area is defined as:

$$F_i^n = S_i^n - \overline{S_i^n} \quad \text{for } i = 1,...,N,$$

where $\overline{S_i^n} = \frac{1}{13}\sum_{j=i-6}^{i+6} S_j^n$. Each of $\{F_i^n\}_{i=1}^{N}$ and $\{F_{i=1}^s\}_{i=1}^{N}$ contains $N = 142$ elements.

To investigate the behavior of the mid-term periodicity in longitude zones the mean position and the total area of each sunspot group cluster or each single groups during each Carrington rotation of the cycle 19 evaluated by Getko (2013) are used. Such data sets from each solar hemisphere are applied to find the best division of solar longitudes into the 30°-wide longitude bins from each solar hemisphere separately and, consequently, to detect longitude zones in which the mid-term periodicities exist.

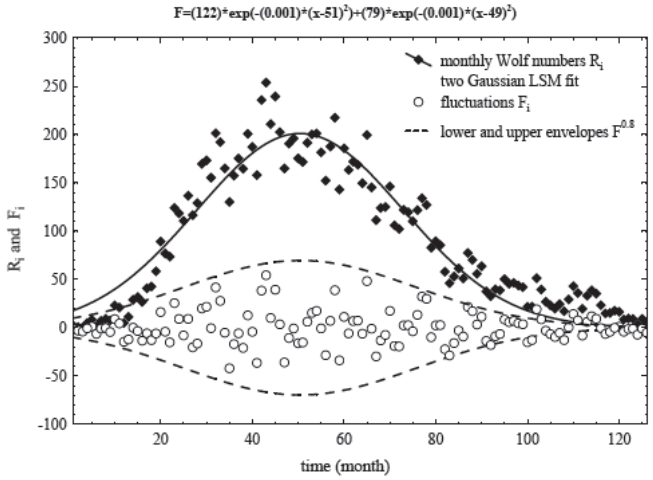


*Figure 3.* The fit of the monthly Wolf numbers $(R_i)$ by the linear combinations of two Gaussian curves (solid line) and the lower and the upper envelopes of the Wolf number fluctuations $(F_i)$ (dashed lines).

## 3. Results

### 3.1 THE MONTHLY WOLF NUMBERS

To find periodicities in the time series $\{F_i\}_{i=1}^{M}$ three functions are used: the auto-correlation function $(c_\tau)$, the periodogram $(p(\tau))$ and the wavelets $(w(t,\tau))$, where $\tau$ is a period and *t* is a time. There is a strong relationship between these functions. For a stationary time series with zero mean the Fourier transform is equivalent to the cosine transform of an auto-correlation

function (Anderson, 1971). When $M \to \infty$ both the functions give the same periodicities. However, for $M < \infty$ both the functions have different properties. When the time series contains a periodicity at $\tau_1$, the auto-correlation function has no local maxima in the interval of $(0, \tau_1)$, and has a global maximum at $\tau_1$

l

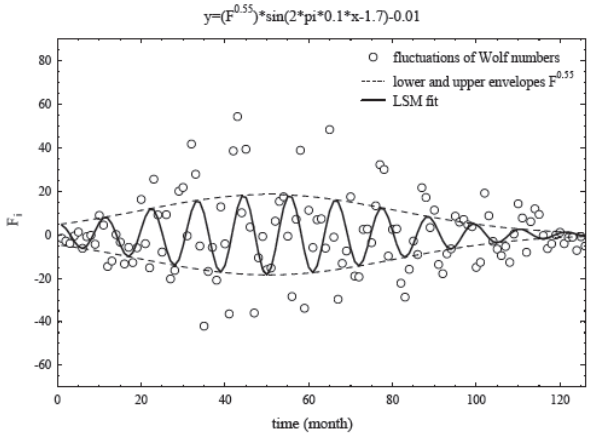


*Figure 4.* The fit of the monthly Wolf numbers ($R_i$) by the linear combinations of two Gaussian curves (solid line) and the lower and the upper envelopes of the Wolf number fluctuations ($F_i$) (dashed lines).

and local maxima at $2\tau_1, 3\tau_1, \ldots$ The periodogram has also a global maximum at $\tau_1$, local maxima at $2\tau_1, 3\tau_1, \ldots$ and additionally at $\frac{1}{2}\tau_1, \frac{1}{3}\tau_1, \ldots$ When the time series contains multiple periodicities, the auto-correlation function has no local maxima in the interval of $(0, \tau_k)$ where $\tau_k$ is the shortest period, but the periodogram can have many artificial peaks in this interval. Thus, to detect periodicities, the highest periodogram peaks for which the auto-correlation function is significantly positive is chosen. The Morlet normalized wavelets with the standard assumption $2\pi\omega = 6$ can also give the periodicities (Torrence and Compo, 1998). The results of the power spectrum and the global wavelet spectrum should be consistent. Figure 1 shows the auto-correlation function and the periodogram of $\{F_i\}$. Both the functions give statistically significant peaks at about 11 months (12 rotations). However, although the 11-month quasi-periodicity dominates the integrated wavelet spectrum (Figure 2b), the significant values in the wavelet map (Figure 2a) are for the increasing-activity period only.

Because the Wolf number fluctuations are weakly correlated $(\rho \approx 0.2)$, the wavelet results can be confirmed by the Least Square Method (LSM). The temporal behavior of cycle 19 can be represented by a linear combination of two Gaussian curves:

$$f(R_i) = d * \exp(-a * (R_i - b)^2) + e * \exp(-a * (R_i - c)^2).$$

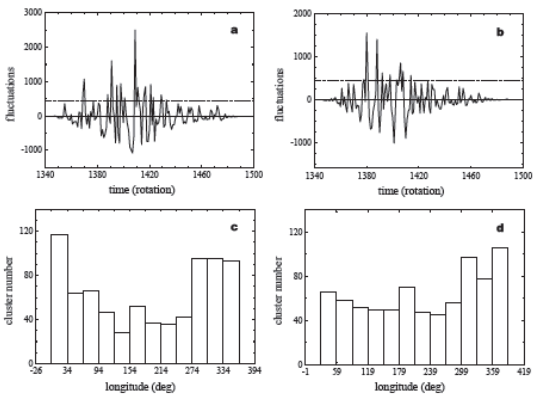


*Figure 5. The left column:* a: Fluctuations of sunspot areas from the northern hemisphere ($\{F_i^n\}_{i=1}^N$). The horizontal solid line shows the zero level. The dashed line represents $1\sigma$ level ($F_i^n > 1\sigma$ indicates the strong fluctuations). c: The best histogram of sunspot group clusters from the northern hemispehere calculated for clusters existed during the strong sunspot area fluctuations. *The right column:* the same as in the left column, but for the southern hemisphere.

The estimated curve $f(R_i)$ is given in Figure 3. The 90% of the variability of $R_i$ is explained by the regression. The Least Square Method (LSM) is applied to estimate the best envelopes of fluctuations $F_i$. An example of such curves are presented in Figure 3. These curves determine the change in the amplitude fluctuation during the solar cycle and
allow to estimate the sine function with a variable amplitude. This function has the following form:

$$y(F_i) = [f(R_i)]^k * \sin(2 * \pi * a_1 * F_i + a_2) + a_3.$$

The points $(i, F_i)$ and the best fitting sine line (with the period of 11 months) delimited by the lower envelope $-[f(R_i)]^{0.55}$ and the upper envelope $[f(R_i)]^{0.55}$ are shown in Figure 4. To test the regression, the F-statistic is used. The null hypothesis $H_0: \; k = a_1 = a_2 = a_3 = 0$ is rejected because $F_{(3,122)} \approx 10.3 >> F_{(3,122)}(\alpha = 0.05) \approx 2.74$.
However, the analysis of variance indicates that the 38% of the variability of $y(F_i)$ is explained by the regression model only. This confirms the wavelet results that it is difficult to conclude that the 11-month periodicity exists during the entire data set.

## 3.2 THE SUNSPOT AREAS PER ROTATION

Similar analysis was done for the sunspot area fluctuations from each solar hemisphere separately. For the northern hemisphere the auto-correlation function has a local maximum at $\tau = 11$ rotations which is greater than $1\sigma$, but the periodogram and the global wavelet spectrum have the global maxima at about 10 rotations. The wavelet map shows statistically significant peak at $\tau \approx 10$ rotations. It is extended in

time up to 17 rotations during the increasing-activity period and dominates the integrated spectrum.

The southern hemisphere analysis leads to similar conclusions. The auto-correlation function has two statistically significant peaks at $\tau \approx 8$ and 10 rotations. The periodogram and the global wavelet spectrum have global maxima at about 9 rotations, but the wavelet maps shows two statistically significant islands of power during the increasing-activity period which exist 23 rotations together.

To combine the wavelet results with the observed features on the solar surface, the longitude zones of sunspot-group clusters that create the strong sunspot area fluctuations from each solar hemisphere are evaluated. This method was introduced by Getko (2014). Firstly, for each case a set of strong positive fluctuations is defined. Because the empirical distributions of each fluctuation time series is not normal, the $3\sigma$ rule should not be used. Thus, a method that supplies the best value of the parameter *p* such that the fluctuation (for example, for the northern hemisphere) $\boldsymbol{F_i > p}$ could be treated as a strong fluctuation is applied (Getko, 2004). It is $1\sigma$, where $\sigma$ is the empirical standard deviation of each fluctuation time series. Next, for each i-th rotation (such that $\boldsymbol{F_i^n > p}$) the mean positions and the rotational sum of each sunspot group areas are calculated and all clusters created by large groups and all smaller groups that are close to one another are found (Getko, 2014). For such clusters, the weighted positions of the area and total areas are evaluated. Almost all clusters have a longitudinal extent up to 30° (Getko, 2007). To obtain their longitude distribution, the solar disk is divided into 30°-wide longitude bins. For each bin the number of clusters is determined. To avoid a phase shift problem, thirty histograms such that their first bin started from 0° to 29° every 1° are taken into consideration. For each of them the sum of the squares of the deviations of the empirical frequencies from the uniform-distribution values is calculated. For the best histogram this sum is to be greater than from any other histogram. Figures 5a and 5b demonstrate the sunspot area fluctuations $\boldsymbol{\{F_i^n\}}$ and $\boldsymbol{\{F_i^s\}}$. The dashed horizontal line indicates the level $\boldsymbol{p}$ which evaluates the strong positive fluctuations. Figures 5c and 5d show the best histogram of sunspot group clusters which create the strong positive fluctuations for each hemisphere respectively. Such a longitude separation provides the 12 time series each of which contains the total areas of all the clusters and all other sunspot groups (which do not create clusters) occurring in the 30° bin. To find the mid-term periodicities for each longitude bin, the wavelets of sunspot areas are applied. Figures 6 - 9 contain the wavelet maps of sunspot areas in the northern hemisphere from the longitude bins: 274° – 304°, 304° – 334°, 334° – 4° and 4° – 34° respectively. The same show Figures 10 - 13, but for the southern hemisphere from the longitude bins: 299° – 329°, 329° – 359°, 359° – 29° and 29° – 59° respectively. As seen in these Figures it is difficult to find one dominant periodicity that is common for all cases. It is rather a set of periodicities which dominate the integrated spectrum and exists in wavelet maps as the islands of power during the part of solar cycle. The set of mid-periodicities is divided into two parts: around 10 rotations

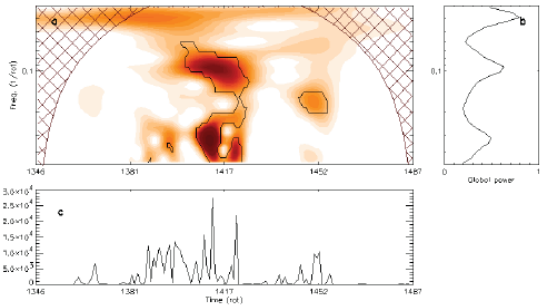

*Figure 6.* The same as in Figure 1, but for the sunspot area fluctuations $\{F_i^n\}_{i=1}^N$ from the longitude bin 274° – 304°.

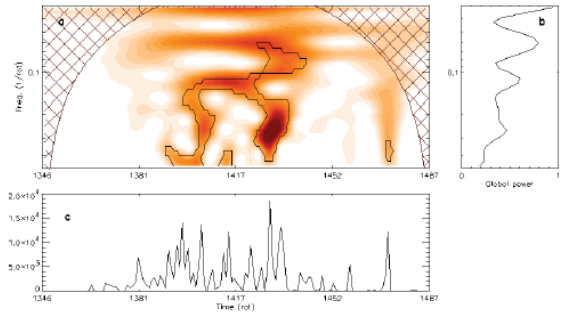

*Figure 7.* The same as in Figure 1, but for the sunspot area fluctuations $\{F_i^n\}_{i=1}^N$ from the longitude bin 304° – 334°

(from the interval of [7, 14] rotations) and around 6 rotations (from the interval of [4, 7) rotations). Such a division was demonstrated by Getko (2009} because of the auto-correlation analyses of sunspot area fluctuations from 12 solar cycles in each solar hemisphere separately.

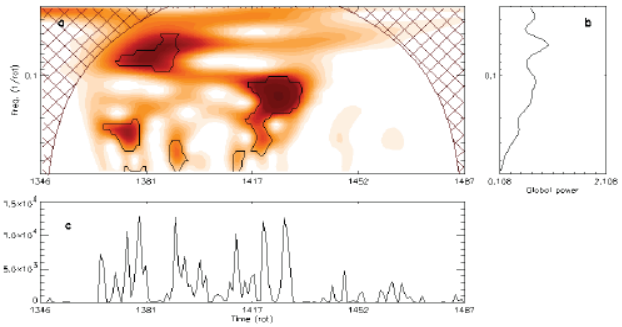

*Figure 8.* The same as in Figure 1, but for the sunspot area fluctuations $\{F_i^n\}_{i=1}^N$ from the longitude bin 334° – 4°

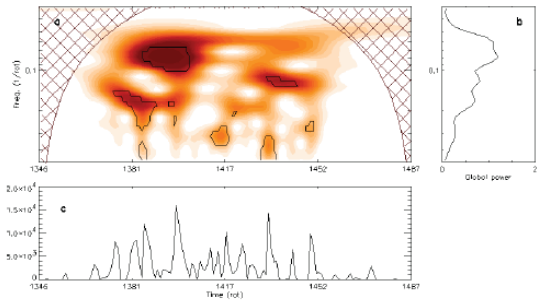


*Figure 9.* The same as in Figure 1, but for the sunspot area fluctuations $\{F_i^n\}_{i=1}^N$ from the longitude bin $4° - 34°$

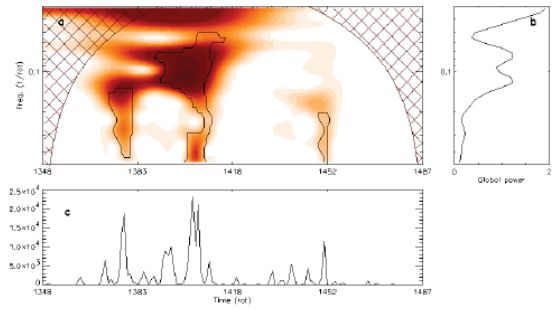


*Figure 10.* The same as in Figure 1, but for the sunspot area fluctuations $\{F_i^s\}_{i=1}^N$ from the longitude bin $299° - 329°$.

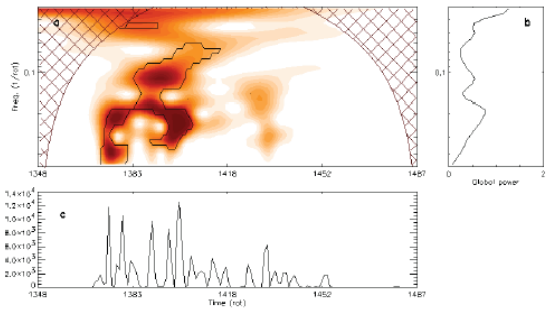


*Figure 11.* The same as in Figure 1, but for the sunspot area fluctuations $\{F_i^s\}_{i=1}^N$ from the longitude bin $329° - 359°$

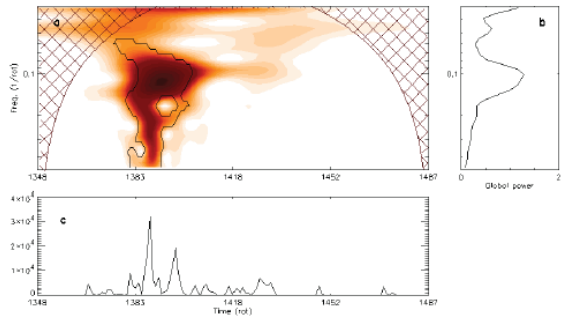


*Figure 12.* The same as in Figure 1, but for the sunspot area fluctuations $\{F_i^s\}_{i=1}^N$ from the longitude bin $359° - 29°$

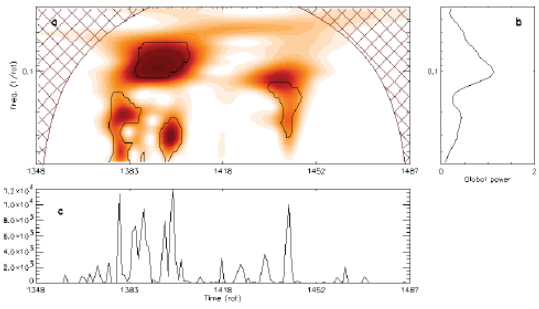


*Figure 13.* The same as in Figure 1, but for the sunspot area fluctuations $\{F_i^n\}_{i=1}^N$ from the longitude bin $29° - 59°$

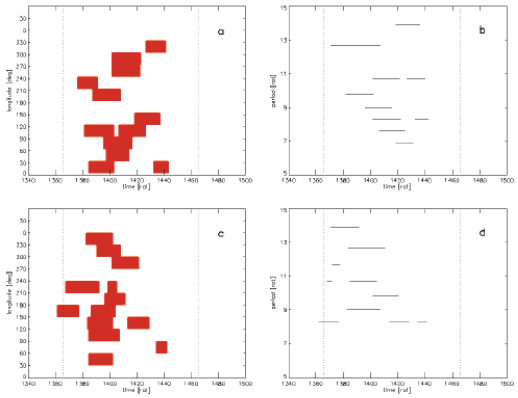


*Figure 14. The upper row:* a: Filled red areas demonstrate the presence of the northern hemispheric 10-rotation quasi-periodicity in 30°-wide longitude bins during cycle 19. Vertical dotted lines show the high- and the low-activity periods. b: Behaviour of the northern hemispheric 10-rotation quasi-periodicity. Vertical dotted lines show the high- and the low-activity periods. *The lower row:* The same as in the upper row, but for the southern hemisphere.

Figures 14b and 14d show the behavior of the 10-rotation quasi-periodicities from the northern and the southern hemispheres respectively. Vertical dotted lines show the high-
and the low-activity periods. In Figures 14c and 14d filled red areas demonstrate the presence of the 10-rotation quasi-periodicity in 30°-wide longitude bins from the northern
and the southern hemispheres respectively. Vertical dotted lines show the high- and the low-activity periods. The same, but for the 6-rotation quasi-periodicity is presented in Figures 15.

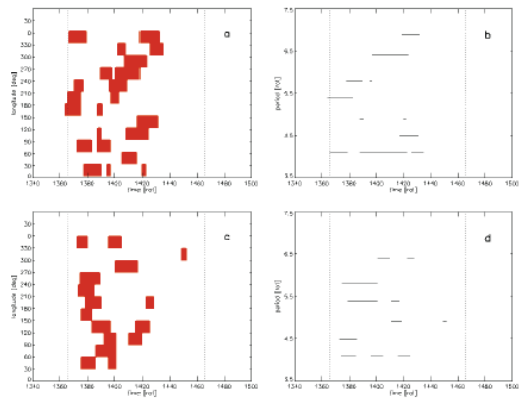


*Figure 15.* The same as in Figure 14, but for the 6-rotation quasi-periodicity.

## 4. Conclusions

The following results have been obtained:

(i) The spectral and the auto-correlation analyses of Wolf number fluctuations for the most active solar cycle (cycle 19) show that the average length among fluctuation maxima is about 11 months (12 rotations). The global wavelet power of these fluctuations confirms this result.

(ii) The best-fitting for Wolf number fluctuations indicates that only about 40% of the fluctuations variance is explained by regression. This percentage increases when the contribution of the positive fluctuations increases (from 40% for the same weights for positive and negative fluctuations to 50% for the regression calculated for positive fluctuations only). Thus, it is difficult to assume that the detected 11-month periodicity exists in the entire data set.

(iii) The local wavelet map of Wolf number fluctuations presents the existence of short-lasting oscillations with the period about 11 months during the increasing-activity period.

(iv) The wavelets of sunspot area fluctuations from each solar hemisphere show the statistically significant values at about 10 rotations. These quasi-periodicities exist about 27 rotations during the high-activity period in each solar hemisphere and dominate the integrated spectra.

(v) The division of each solar hemisphere into $30^{o}$-wide longitude bins and the wavelet calculations for the areas of sunspot clusters belonging to these $30^{o}$ bins enable one to detect from 1 to 3 quasi-periodic longitude zones at the same time which show the 10-rotation quasi-periodicity. They always present during the high-activity period (73 rotations for the northern hemisphere and 81 rotations for the southern hemisphere).

(vi) It is difficult to find one or more quasi-periodic longitude zones which exist during the whole solar cycle.

(vii) The 6-rotation quasi-periodicity (from 4 to 7 rotations) is also detected, but the global wavelet powers calculated for quasi-periodical longitude zones show small local maxima. The wavelet maps indicate that the peaks for this periodicity are often weaker than these for the 10-rotation quasi-periodicity. Moreover, the time intervals where they exist are much shorter.

**References**


Anderson, T. W.: 1971, The Statistical Analysis of Time Series, John Wiley and Sons, New York.

Getko, R.: 2004, Solar Phys. 224, 291. doi:10.1007/s11207-005-5718-7.

Getko, R.: 2006, Solar Phys. 238, 187. doi:10.1007/s11207-006-0112-7.

Getko, R.: 2007, Adv. Space Res. 40, 981. doi:10.1016/j.asr.2007.02.094.

Getko, R.: 2009, in: Gopalswamy, N., Webb D., (eds.) Universal Heliophysical Processes, IAU Symp. 257, Cambridge University Press, 169. doi:10.1017/S174392130902924X.

Getko, R.: 2013, J. Space Weather Space Clim. 3, A09. doi:10.1051/swsc/2013032.

Getko, R.: 2014, Solar Phys. 289, 2269. doi:10.1007/s11207-013-0447-9.

Obridko, V. N., Shelting, B.D.: 2007, Adv. Space Res. 40, 1006. doi:10.1016/j.asr.2007.04.105.

Torrence, C., Compo, G. P.: 1998, Bull. Am. Meteor. Soc. 79, 61.

Vizoso, G., Ballester, J. L.: 1990, Astron. Astrophys. 229, 540.